First European Conference on Earthquake Engineering and Seismology
(a joint event of the 13th ECEE & 30th General Assembly of the ESC)
Geneva, Switzerland, 3-8 September 2006
Paper Number: Keynote Address K1b

EARTHQUAKE DYNAMICS AND THE PREDICTION OF STRONG GROUND MOTION

Raul MADARIAGA[1]

SUMMARY

A large number of earthquakes have been modelled in detail using seismological, geological and geodetic information. Several common traits have been found for earthquakes kinematics at periods longer than 3s. At these frequencies, all large earthquakes (M>7) appear complex with highly variable slip, and propagate with rupture velocities close to about 80 % of the shear wave speed. Starting from these kinematic inversions, it is possible to use numerical wave propagation models in order to estimate the complete radiated field including near and far field effects. Radiation can be separated into two main components: a near field term responsible for the so-called fling steps due to permanent, geodetic offsets; and the far field that produces pulse like motions. Using seismological scaling relations it is possible to explain the main features of displacement spectra using classical seismological models at long periods. Seismic simulations may now be extended to the frequencies up to a few Hz by means of dynamic rupture propagation, where rupture is simulated starting from the kinematic models. In this talk I will review the main results obtained so far and the new avenues of research that have been opened thanks to new near field earthquake data and the ability to simulate increasingly complex and realistic seismic ruptures in a computer.

1. INTRODUCTION

Earthquake source dynamics provides key elements for the prediction of strong ground motion. Actually, the original circular crack model of Madariaga (1976) was developed in order to understand the spectral model proposed by Brune (1970). Early studies pioneered our understanding of friction and introduced simple models of dynamic earthquake rupture, typically using homogeneous distributions of stress and friction parameters. Among the best known of those models are the rectangular dislocation proposed by Haskell (1964) and the self-similar circular rupture model introduced by Kostrov (1966). Extensive research then followed in order to advance our understanding of seismic rupture propagation and seismic wave radiation. Very soon it became clear that the classical model of a sudden drop in friction from a static to a dynamic coefficient was inadequate because it produced in finite stress singularities. The reason is that friction laws require a length scale in order to produce a finite energy release rate near the rupture front. The first model with a proper friction law was proposed by Ida (1982) who introduced the term slip weakening model. This friction model was adopted by Andrews (1976a, b) for the study plane ruptures and by Day (1982) for 3D fault models. These authors showed that slip weakening regularizes the numerical model of the rupture front, distributing stress and slip concentrations over a distance controlled by the length scale in the friction law. Extensive reviews on rupture dynamics until 1990 were published by Kostrov and Das (1989) and Scholz (1989).

Recent studies of rupture processes for selected earthquakes have shed new light on our understanding of earthquake ruptures. These models suggest a complexity of the rupture process that the early models of rupture in a uniformly loaded medium were unable to explain. By the end of the 80s good quality near field accelerometers became available for some large earthquakes; and, simultaneously, new sophisticated and

[1] Laboratoire de Géologie UMR CNRS 8538, Ecole Normale Supérieure, 24 rue Lhomond, 75231 Paris Cedex 05, France,
Email : madariag@geologie.ens.fr

efficient numerical methods provided the tools to study realistic dynamic rupture propagation. Heaton (1990) noticed that rupture of large earthquakes was typically characterized by pulse-like behaviour, where only a small part of the fault would rupture at a given instant. This observation has been confirmed by a number of inversions of large earthquakes, such as the 1992 Landers earthquake (Wald and Heaton, 1994; Cohee and Beroza, 1994; Cotton and Campillo, 1995). Olsen et al. (1997) and Peyrat et al (2001) showed that rupture propagation in the 1992 Landers, California earthquake, followed a complex path, completely controlled by the spatial variation of the initial stress field. Ide and Takeo (1997) estimated the constitutive friction law parameters for the 1995 Kobe earthquake from their kinematic inversion results. Computations of dynamic stress changes for the 1992 Landers, 1994 Northridge, and 1995 Kobe earthquakes (Bouchon, 1997) showed highly variable distributions of stress drops. In this paper we review some important results obtained in the field of earthquake rupture to date.

2. FAULT MODELS AND FRICTION

Let us review the general features of the most common earthquake models. First, those models that emphasize the kinematic description of an earthquake as a propagating rupture: the dislocation model. This model has several unwanted features that affect the radiation of high frequencies. In order to correct them we introduce, in the second part, dynamic earthquake models and some very simple friction laws.

2.1 Dislocation models

In spite of much recent progress in understanding the dynamics of earthquake ruptures, the most widely used models for interpreting seismic radiation are the so-called dislocation models. In these models the earthquake is simulated as the kinematic spreading of a displacement discontinuity (slip or dislocation in seismological usage) along a fault plane. In its most general version, slip may be completely arbitrary and rupture propagation may be as general as wanted. In this version the dislocation model is a perfectly legitimate description of an earthquake as the propagation of a slip episode on a fault plane. It must be remarked, however, that not all slip distributions are physically acceptable: most dislocation models present unacceptable features like interpenetration of matter, release unbounded amounts of energy, etc. For these reasons dislocation models must be considered as a useful intermediate step in the formulation of a physically acceptable dynamic fault model.

Dislocation models are very useful in the simulation of near field accelerograms (see, e.g. Wald and Heaton, 1994; Cohee and Beroza, 1994; Cotton and Campillo, 1995 and many others). Radiation from a dislocation model can be written as a functional of the distribution of slip on the fault. In a simplified form a seismogram u(x, t) at an arbitrary position x can be written as:

$$u(x,t) = \int_S \int_0^\infty D(\xi,\tau) G(x,t;\xi,\tau) d\xi d\tau \qquad (1)$$

Where S is the surface of the fault, $G(x, t; \xi, \tau)$ is the Green tensor that may be computed using simple layered models of the crustal structure, numerical simulations or by the so-called empirical method that consists in using smaller events as Green functions. In (1) slip

$$D(x,t) = u(x^+,t) - u(x^-,t) \qquad (2)$$

is defined as the jump in displacement between the positive and the negative side of the fault. The notation $x^\pm$ indicates a point immediately above or below the fault.

2.2 Dynamic models

Let us now study the main features of a seismic source model in an isotropic elastic model of the earth. Inside the elastic medium seismic propagation obeys the equation of linear elastodynamics. Once rupture starts, displacement and particle velocities become discontinuous across the fault. Slip D produces changes in the state of stress on the fault and in the elastic medium surrounding it. This change in stress may or may not be compatible with some basic mechanical laws, like energy conservation, continuity of matter, etc. For this reason it is necessary to take into account the friction law that that acts between the two sides of the fault.

$$T(D,\dot{D},\theta) = T_{total} \qquad (3)$$

Friction T is a function of slip D, slip rate D and several state variables denoted by θ. The traction that appears in friction laws is the total traction T_{total} on the fault which can be expressed as the sum of a pre-existing stress $T_0(x)$ and the stress change ΔT due to slip. The pre-stress is caused by tectonic load of the fault and the residual stress field left over from previous seismic events on the fault or its immediate vicinity.

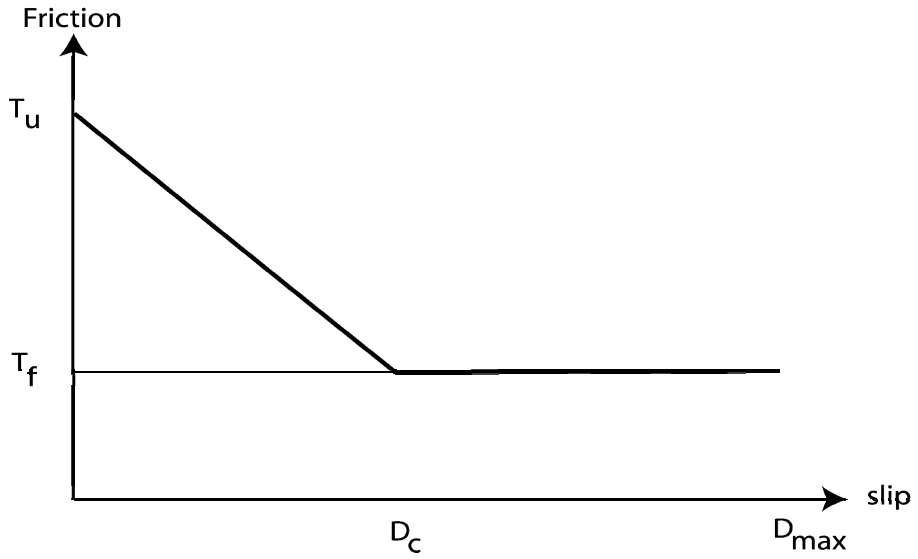

Figure 1: Slip and slip-rate dependent friction law. For values of stress less than the peak static friction (T_u), slip is zero. Once slip begins, stress decreases as slip increases until slip has reached the limit *Dc*. Once slip is larger than the slip weakening distance D_c, friction remains constant at a residual value T_f. The final slip in this model is defined by D_{max}.

Friction laws can be quite complex depending on slip rate and the state of the interface. Here we will discuss the simple slip weakening friction law introduced by Ida (1972). This friction law shown in Figure 1 is an adaptation to shear faulting of the Barenblatt-Dugdale friction laws used in hydro-fracturing and tensional (mode I) cracks. In this friction law, slip is zero until the total stress reaches a peak value (yield stress) that we denote with T_u. Once this stress threshold has been reached, slip D starts to increase from zero and $T(D)$ decreases linearly to T_f as slip increases:

$$\begin{aligned} T(D) &= T_u\,(1 - D/D_c) + T_f \quad \text{for} \quad D < D_c \\ T(D) &= T_f \qquad\qquad\qquad\quad \text{for} \quad D \geq D_c \end{aligned} \tag{4}$$

where D_c is a characteristic slip distance and T_f is the residual friction at high slip rate, sometimes called the kinematic friction. The slip weakening friction law (4) has been used in numerical simulations of rupture by Andrews (1976a,b), Day (1982b), Fukuyama and Madariaga (1998), Madariaga et al (1998), and many others. Most recent work on friction has concentrated in a class of friction laws that depend both on slip rate and state variables. These laws were developed from laboratory experiments at low slip rates by Dieterich (1978) and Ruina (1983). We are not going to discuss them any further here, because as shown by Bizzarri et al (2001), at high enough slip rates there is no significant difference between slip weakening and the simpler slip weakening law (4). Although rate and state dependent friction are very important for the study of rupture initiation and repeated ruptures on a fault surface, its features are indistinguishable from simpler slip weakening friction laws during the dynamic part of seismic ruptures.

3. NUMERICAL MODELLING OF SEISMIC RUPTURES

With the rare exception of a few very simple kinematic fault models embedded in a homogeneous elastic medium, it is virtually impossible to obtain analytical expressions for the seismograms produced by seismic ruptures. Numerical methods are required for even the simplest circular fault models. Many methods have been used in the literature including semi-analytical approaches for simple sources in layered media (Bouchon et al, 1984), and full numerical techniques for more complex source models and elastic media. Let us briefly review those numerical techniques.

3.1 The Boundary Integral Element (BIE) Method

The BIE method consists in solving the elastic wave equation semi analytically by the Green's functions method. Then these Green's functions are used to compute stresses for an arbitrary distribution of slip. The slip is found using the frictional boundary condition (4). In the original version of the BIE method, proposed by Das and Aki (1977) the equation was solved in terms of stresses. This technique was extended to 3D by Das (1980) and improved by Andrews (1985). An alternative version of the BIE method, the so-called indirect or displacement discontinuity method was proposed by Koller et al (1972). The indirect method was improved by the removal of strong singularities by a number of authors (e.g., Cochard and Madariaga, 1994; Fukuyama and Madariaga, 1998). All current formulations of the BIE method have been developed for faults of different shapes embedded in homogeneous elastic media. The reason is that the Green function can be computed analytically only in very simple media. The BIE method is the only technique that can deal efficiently with segmented faults embedded in 3D media. Unfortunately, for the moment the fault has to be embedded in a homogeneous elastic media.

3.2 The Finite Difference (FD) Method

The other numerical method widely used for the simulation of dynamic and kinematic sources is the finite-difference (FD) method. This method was introduced by Andrews (1976) and Madariaga (1976) for the study of seismic ruptures and developed by numerous authors (e.g., Day, 1982; et al., 1997; Madariaga et al., 1998). Numerous implementations of the FD method have been presented in the literature but most recent work is based on the staggered-grid discretization of the mixed velocity-stress formulation of the wave equation. Olsen et al. (1995) used this method to compute wave propagation around a kinematically defined rupture in a large-scale 3D model. Another important difference between implementations of FD are in the way boundary conditions are handled. Some authors, like Madariaga et al. (1998) use the so-called “thick fault” boundary conditions where the fault is actually represented by its moment tensor density. Another popular method is to create a real fault by "splitting the nodes" on the two sides of the fault. Although the two techniques may be more efficient for certain problems the differences are actually minor (see a discussions by Andrews, 1999; or Day et al, 2005).

3.3 Finite elements and Spectral elements

The classical finite element method with low order interpolation functions has been used by several authors to model earthquake kinematics and dynamics. The results are not excellent because in the FEM, stresses by construction are lower order than displacements. The frictional boundary condition involves functions of different polynomial order, so that the fit of the friction law is usually noisy. The standard procedure is to reduce the noise by some filter like numerical dissipation. In recent years, much more efficient formulations based on the split-node techniques have appeared, with noise control at the boundary. Another approach that gives excellent results is to use higher order finite elements together with split nodes. It is then possible to satisfy the boundary conditions using local filters to reduce noise. A novel FE technique has been recently introduced in geophysics by Komatisch and Vilotte (1988), the so-called spectral element method. This is a variation of the FEM using a base of orthogonal interpolation functions. This method is more expensive that classical finite elements and finite differences, of course, but it has much better accuracy. It is very likely that high order FE methods will replace finite differences in the long run, because spectral elements can be used to simulate segmented non-planar faults embedded in irregular media (see Madariaga and Ampuero, 2005). SEM's do also an excellent job at modelling free surface effects, precisely where finite differences are very inaccurate.

3.4 Dimensional Analysis

Proper formulation of numerical methods for simulating earthquakes and computing seismic radiation requires some basic understanding of scaling. This also has the advantage of clearly showing how to properly discretize the wave equation so as to minimize dispersion and avoid numerical instability. We choose the following dimensional variables:

• Distances along the fault are measured in units of Δx, the grid interval.
• Wave velocities are measured in units of β, the shear wave velocity.
• Stress is measured in units of stress drop $(T_u - T_f)$.

All other dimensions are determined by the previous three. In particular, the time step is determined by

$$H = \frac{\alpha \Delta t}{\Delta x} \quad (5)$$

where α is the compressional wave speed. H is the so-called CFL (Courant-Friedrich-Lewy), a non-dimensional number that controls the stability of time integration in numerical method. In our simulations it was usually taken as 0.30 in order to insure stability and good accuracy.

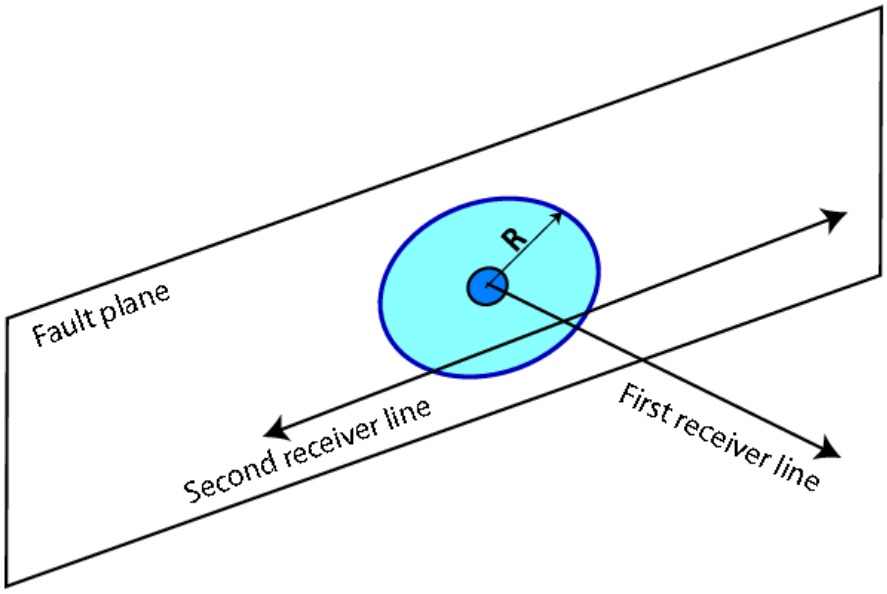

Figure 2: The circular crack model we model dynamically. Rupture starts from a small patch located near the centre of the fault. Rupture is contained inside the circular fault zone by an unbreakable barrier of radius R = 12 km. The lines indicate the position of the recording sites shown in Figures 5 and 6.

An essential requirement for an accurate numerical method is that the solution becomes independent of grid size beyond the use of a certain number of grid points per wavelength. The shortest physical length in a dynamic simulation is the width of the rupture front that can be computed from the slip-weakening distance Dc as shown by Ida (1972), Andrews (1976) and Day (1982b). For 2D faults and for the slip weakening law (4) this width, *Lc* can be computed from

$$\kappa = \frac{(T_{\text{ext}} - T_{\text{f}})^2 L_c}{\mu (T_u - T_f) D_c} \quad (6)$$

where κ is a non-dimensional number of order 1 that controls rupture triggering and propagation. It depends on the dimensions of the problem and on details of the geometry. In order for the numerical method to converge we define an additional numerical ratio

$$R_c = \frac{L_c}{\Delta x} \quad (7)$$

that is the number of grids in the process zone near the rupture front. From a close examination of a large number of numerical simulations, Madariaga et al (1998) concluded that proper numerical simulations require that Rc > 7. For 3D simulations, this is a rather large number that requires the use of very dense grids for accurate simulation of spontaneous rupture.

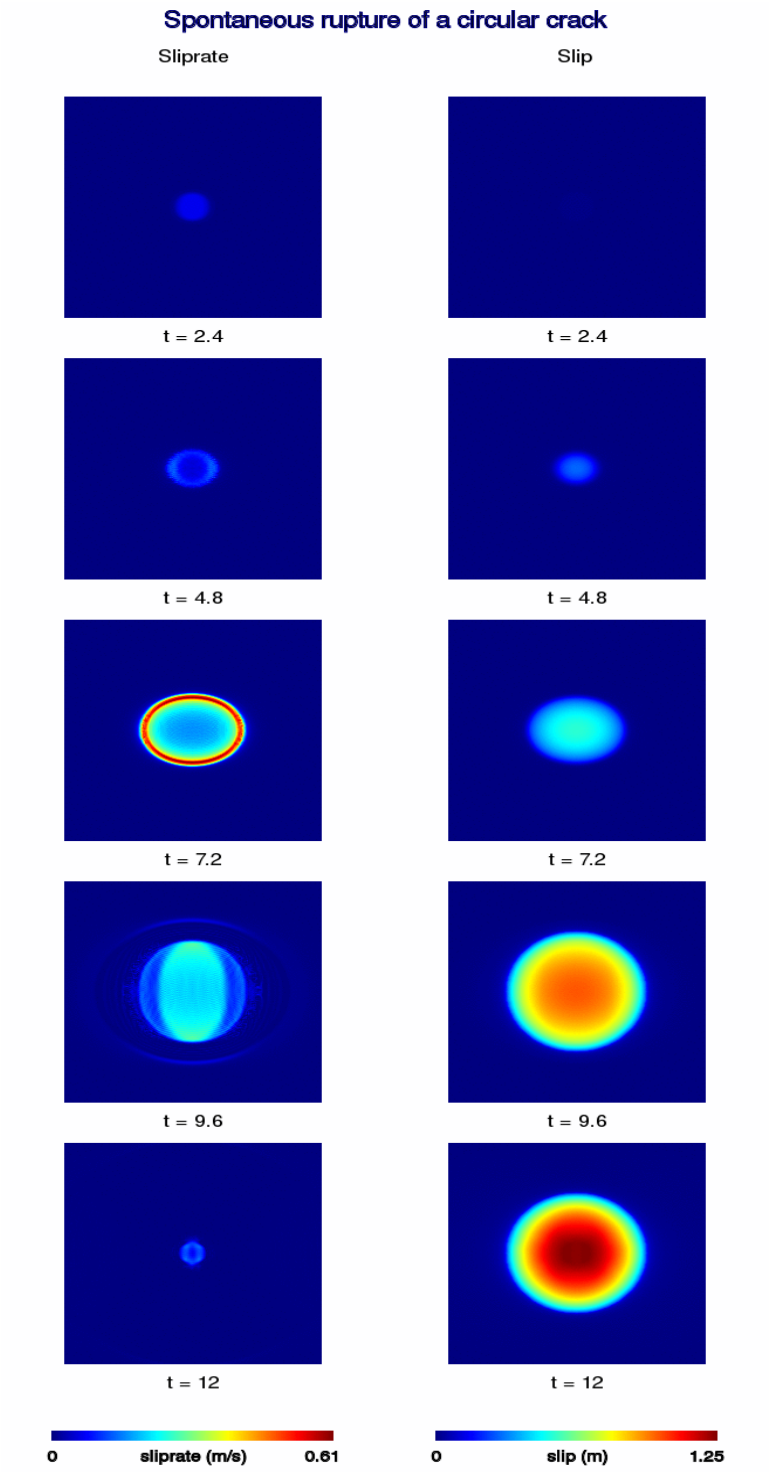

Figure 3: Slip rate and slip distribution on the fault plane for the circular crack model. Each snapshot represents the slip rate or slip distribution at an instant of time. The colour scale is at the bottom of each column. The snapshots are plotted every 2.4 s starting from 2.4 s at the top down to 12 s at the bottom. The total duration of the rupture process is roughly 10.5 s

4. A SIMPLE CIRCULAR CRACK MODEL

In order to illustrate the main features of dynamic rupture we study a very simple earthquake model inspired by the circular fault model of Brune (1970) and Madariaga (1976). The model we study is appropriate for a magnitude 6.5 event. Instead of a fixed rupture speed as assumed by the latter author, we let rupture propagate spontaneously under the slip-weakening friction law (4). As shown in Figure 2 the fault surface is a plane perpendicular to the z-axis. We assume that the initial stress field on the fault plane is uniform and equal to T_e. For rupture to propagate we need to start it from the centre of the fault reducing the friction over as mall patch of radius Rasp, say. We solve numerically for the spontaneous propagation of rupture using the finite difference method proposed by Madariaga et al (1998). Rupture propagates spontaneously under constant initial stress and friction outside the initial asperity until it finally stops at an unbreakable barrier of radius R. For the numerical computation we will present here we adopted the following numerical values: the medium has a P-wave speed α = 6 km/s, shear wave speed β = 3.465 km/s and density ρ. = 2.67 kg/m^3. The corresponding elastic rigidity is μ = 3.2 × 10^{10} Pa. The spatial step of the finite difference grid was Δx = 200 m and the time step Δt = 0.1 s. With this choice the CFL parameter is H = 0.3, a value that insures both numerical stability and low numerical dispersion.

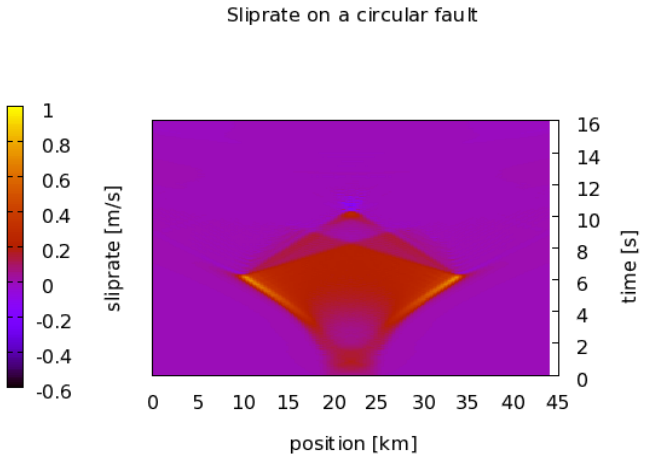

Figure 4: Slip rate as a function of space and time along the x-axis of the fault. Rupture starts from a patch of radius 3 km centred at 22 km. Rupture starts very slowly and picks up speed at around 2 s. Then it ruptures at very high sub shear speeds of the order of 90 % of the shear wave speed. The slip rate concentration at the rupture front reaches 1 m/s. Rupture suddenly stops when the fault reaches a radius of 12 km. P and S stopping phases emitted from the edges of the fault are clearly visible. Slip stops completely at about 12 s.

The uniform initial stress field was assumed to be T_e =5 MPa and the parameters of the slip weakening friction law outside the initial asperity were T_u = 8. MPa, T_f = 0 and D_c = 0.2 m. Without loss of generality we chose T_f =0 because only stress changes matter in dynamic computations. The stress drop $\Delta\sigma = T_e - T_f$ is 5 MPa, a value that is very close to the average observed stress drop for many earthquakes. With these values we find that L_c = 2304 m, and that R_c = 11.5 in (7). Thus the process zone near the rupture front is well resolved in the simulation.
In Figure 3 we show the propagation of rupture on the fault plane as a function of time. In this figure the left column shows the slip rate distribution on the fault at four instants of time, and on the right we plot the slip distribution at the same instants. At time t = 0 rupture is initiated on an initial patch of radius R_{asp} = 3 km and then it propagates outwards as shown in the images for times t > 2:4 s. Rupture stops when it reaches a circular unbreakable barrier of radius R = 12 km. The rupture process is shown in greater detail in Figure 4 that shows the slip rate distribution along the x-axis as a function of position on the fault and time. We observe that during the first two seconds rupture stays inside the initial patch, and then accelerates reaching a high sub-shear speed until it abruptly stops when it reaches the unbreakable barrier of radius 12 km at 6.5 s. At that time the barrier emits two strong stopping phases. The fastest one propagates at the P-wave speed, while the second, stronger phase propagates at a speed close to the Rayleigh wave. Once the latter phase reaches the centre of the fault, slip rate drops to zero very rapidly and the fault heals. The role of the stopping phases in determining the duration of slip on the fault is one of the main features of this model. The other interesting feature is that the shear wave

stopping phase is the strongest and sharpest wave propagating on the fault. This wave controls the high frequency radiation from this rupture model. The low frequencies are controlled by the seismic moment that can be computed from the slip distribution on the fault at the end of our computation. Since the maximum slip, at the centre of the fault, is D_{max} = 1.25 m, the seismic moment is M_o = 1.2 10^{19} Nm, that is the moment of a magnitude M_w = 6.5 earthquake.

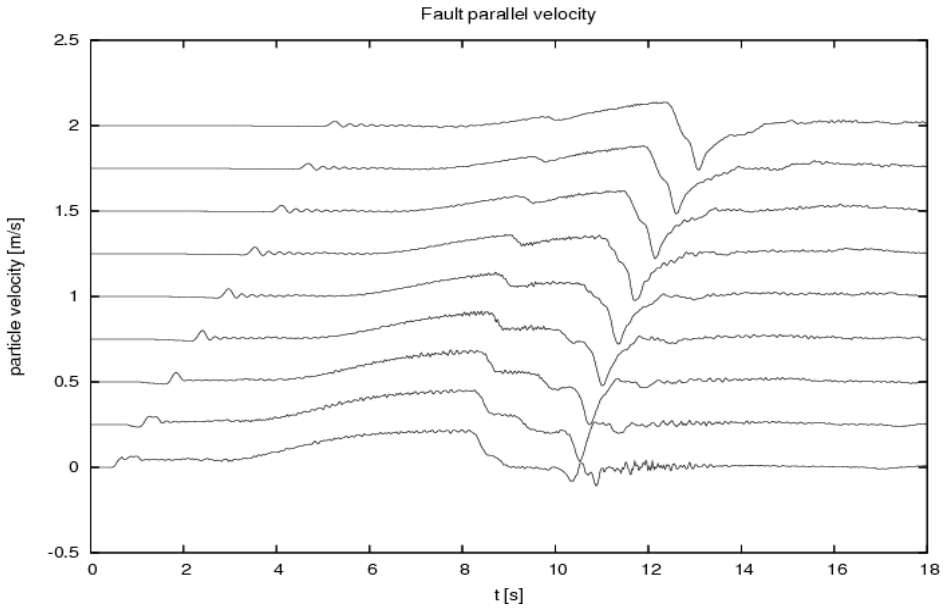

Figure 5: Seismograms along the first receiver line shown in Figure 2. The seismograms plot particle velocity as a function of time. We have added an artificial move out of 0.25 m/s. Seismograms are computed every 2 km along the normal to fault centre. The bottom seismogram is located 2 Km from the fault, the top most 18 km from it.

In Figure 5 we show the seismograms recorded along the first receiver line of Figure 2, this is a line perpendicular to the fault through the centre of the rupture zone. The seismograms show particle velocity as a function of time. In order to show them clearly we added multiples of 0.25 m/s to each successive trace. Some high frequency numerical noise is apparent, but we did not filter it in order to give a clear sense of the accuracy of our simulations. The seismograms were computed at intervals of 2 km starting from the fault itself. The uppermost seismogram is thus located 16 km away from the fault. We observe a clear initiation pulse that propagates away from the fault, then the main starting phase as a slow ramp and finally the larges signal is the stopping phase that is observed at about 10 s in the bottom most seismogram. This Figure shows that the strongest radiation occurs during the stopping phases. In Figure 6 we show the seismograms computed along the second receiver line shown in Figure 2. This line is parallel to the fault at a distance of 8 km from it (the position of the line is shown in Figure 2). The first seismogram at the bottom shows the particle velocity observed at a receiver situated 18 km from the centre of the fault. The following seismograms are plotted at intervals of 4 km so that the topmost one is also 18 km away from the centre of the fault. Seismograms are symmetric about the centre of the fault. Since this figure plots the fault parallel component we observe a decrease in amplitude of the stopping phases away from the centre of the fault.

5. DYNAMIC MODEL OF THE 1992 LANDERS EARTHQUAKE

In the previous section we studied an idealized earthquake of magnitude 6.5, in the present section we consider a real earthquake. The 28 June 1992, magnitude 7.3 Landers earthquake occurred in a remotely located area of the Mojave Desert in Southern California (Figure 7) but the rupture process has been extensively studied due to its large size, proximity to the southern California metropolitan areas, and a wide coverage by seismic instruments. Several studies inverted the rupture history of this event from a combination of seismograms, geodetic and geologic data and the overall kinematics of the seismic rupture are thought to be understood (Wald and Heaton,

1994; Cotton and Campillo, 1995; Cohee and Beroza, 1994) making the Landers earthquake an appropriate test case for dynamic modelling . The work described in this section is a summary of work by Olsen et al. (1997) and Peyrat et al (2001). As observed in Figure 7), the Landers earthquake broke three fault segments: the Landers/Johnson Valley (LJV) segment to the southeast where the hypocenter was located, the Homestead Valley (HV) segment in the central part of the fault, and the Camp Rock/Emerson (CRE) segment to the northwest. For the numerical simulations Olsen et al (1997) replaced the three segments by a single 78-km long vertical fault plane extending from the surface down to 15 km depth.

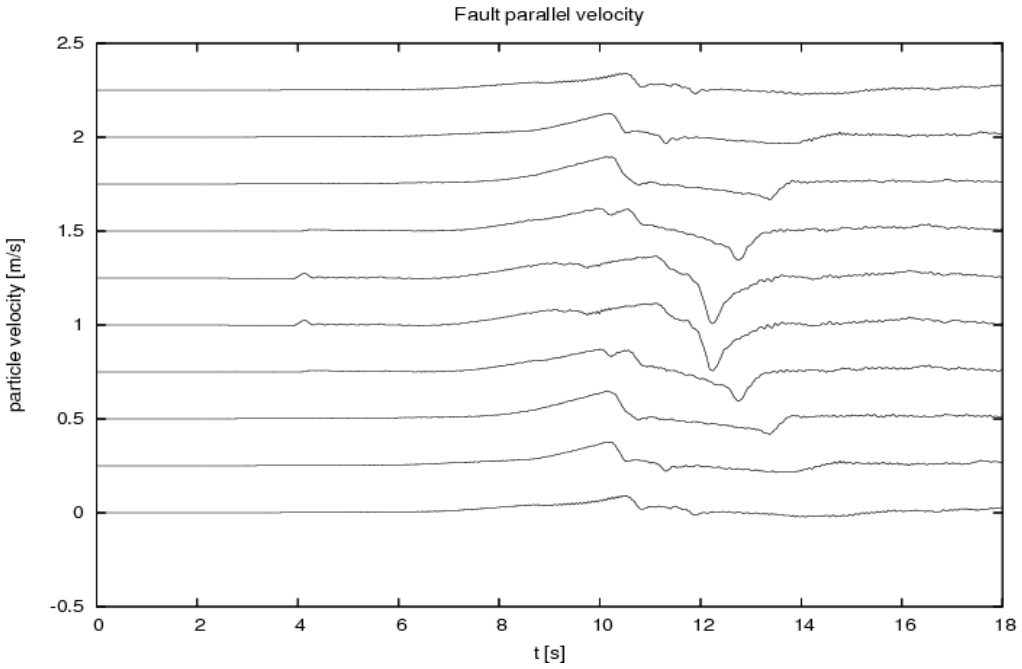

Figure 6: Seismograms along the second receiver line shown in Figure 2. The seismograms plot particle velocity as a function of time. We have added an artificial move out of 0.25 m/s. Seismograms are computed every 4 km along a line parallel to the fault, 4 km away from it. The bottom seismogram is located 18 km from the centre of the fault.

The most important parameter required for dynamic modelling is the initial stress on the fault before rupture starts; all other observables of the seismic rupture, including the motion of the rupture front, are determined by the friction law. An initial stress field was estimated by Olsen et al (1997) from the slip distribution inverted by Wald and Heaton (1994). They computed the stress drop from the slip distribution, and assumed that the initial stress was the sum of a stress baseline of 5 MPa plus the stress drop reversed in sign. In the dynamic inversion, Peyrat et al (2001) used this stress field in order to start the inversion of accelerograms for the initial stress field. It was found that a constant yield stress level T_u = 12 MPa, T_f = 0 MPa and D_c = 0.80 m produces a total rupture time and final slip distribution in agreement with kinematic inversion results. Before the simulation the initial stress T_0 on the fault was constrained to values just below the specified yield level (12 MPa) in order to prevent rupture to start from several locations. In all the simulations we used the same one-dimensional model of velocities and densities as used by Wald and Heaton (1994).

5.1 Rupture Propagation

Rupture was forced to initiate by lowering the yield stress in a small patch of radius 1 km near the hypocenter towards the southern end of the LJV fault strand, as inferred from the kinematic results (Figure 8). Soon after initiation the rupture slows down due to relatively low stress surrounding the initial asperity and shrinks to a small patch of slip near the surface (see snapshots between 3-7 s, Figure 8). Then the rupture enters a high-stress area (7.8 s) about 50 km from the north western edge. At this point the rupture becomes more complex. Part of

the rupture propagates vertically down and stops (7.8-13.3 s, Figure 8), while another part moves laterally close to the surface. The main part of the rupture moves ahead in the general rupture direction where it picks up in strength and enters a high-stress area about 35 km from the north western edge of the fault, representing the HV fault segment. After 14.8 s the rupture spreads to the full width of the fault with the highest intensity near the surface. Here, the rupture pulse resembles the fast, almost instantaneous self-healing phase with a finite slip duration proposed by Heaton (1990) for large earthquakes. At 15.6 s, the rupture enters the CRE segment of the fault, where the rupture extends to greater depths as it propagates with a 'tail' of slowly healing fault material left behind. Towards the north western edge of the fault the rupture leaps ahead for the last time (18.7s) onto a smaller patch of higher-stressed material near the surface. After about 22 s the rupture loses energy and terminates near the upper north western corner of the fault.

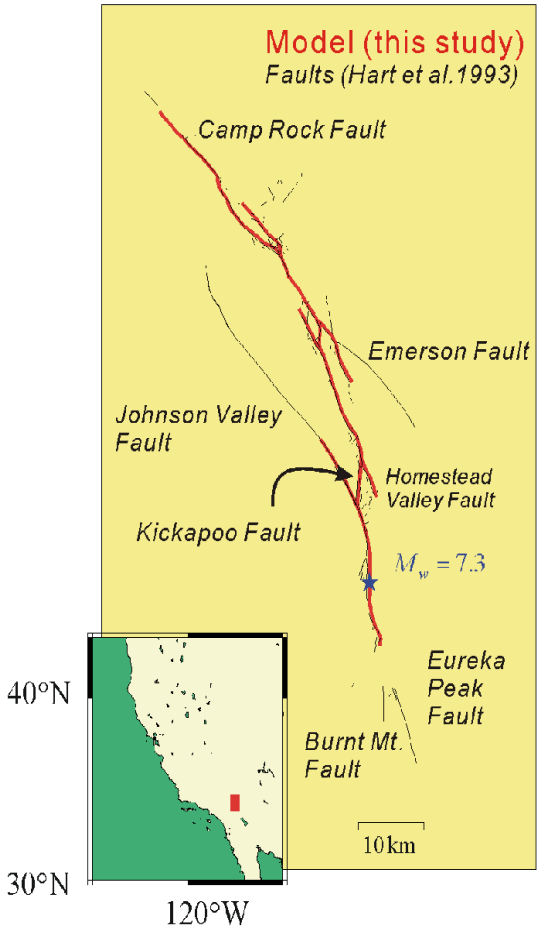

Figure 7: Map showing the surface rupture from the 1992 Landers earthquake. The fault trace is segmented with at least three major sub-faults.

5.2 Inversion of near field data

Peyrat et al (2001) used the strong motion data recorded in the vicinity of the Landers fault to invert for the details of the rupture process. The procedure was one of trial and error. For every initial stress distribution we computed spontaneous rupture process starting from the same initial asperity at the South-western end of the fault. During the iterations, the geometry of the fault and the slip weakening friction law did not change so that T_u = 12 MPa and D_c =0:8 m in all the models we tested. Accelerograms at the recording stations were computed using Bouchon's (1981) frequency-wave number summation method because it is more economical and faster than using finite differences to propagate from the source to the stations. Figure 9 shows a comparison of the synthetic seismograms generated by the best model that Peyrat et al (2001) could find. Both synthetic and

observed seismograms are low-pass filtered to frequencies below 0.5 Hz. The main features of the low-frequency ground motion for amplitude and wave form are reproduced by the synthetic seismograms for the relatively stronger ground motion recorded in the forward rupture direction. The fits for the back-azimuth stations was not as good because the effects of propagation and fault geometry are larger in these stations. The dynamic rupture model of the Landers earthquake is controlled by several friction parameters that are not measured but that may eventually be determined by inversion of seismic and geodetic data. For instance, the rupture speed and healing of the fault are critically determined by the level of the yield stress and the slip weakening distance. If the slip weakening distance is chosen less than about 0.6-0.8 m, the rupture duration and therefore rise times are much shorter than that obtained from kinematic inversion (Wald and Heaton, 1994; Cotton and Campillo, 1995; Cohee and Beroza, 1994). On the other hand, larger values of D_c produce such a strong friction that ruptures do not propagate at all. While the rupture duration and rise times are strongly related to the slip-weakening distance, the final slip distribution remains practically unchanged for slip-weakening distances that allow rupture propagation.

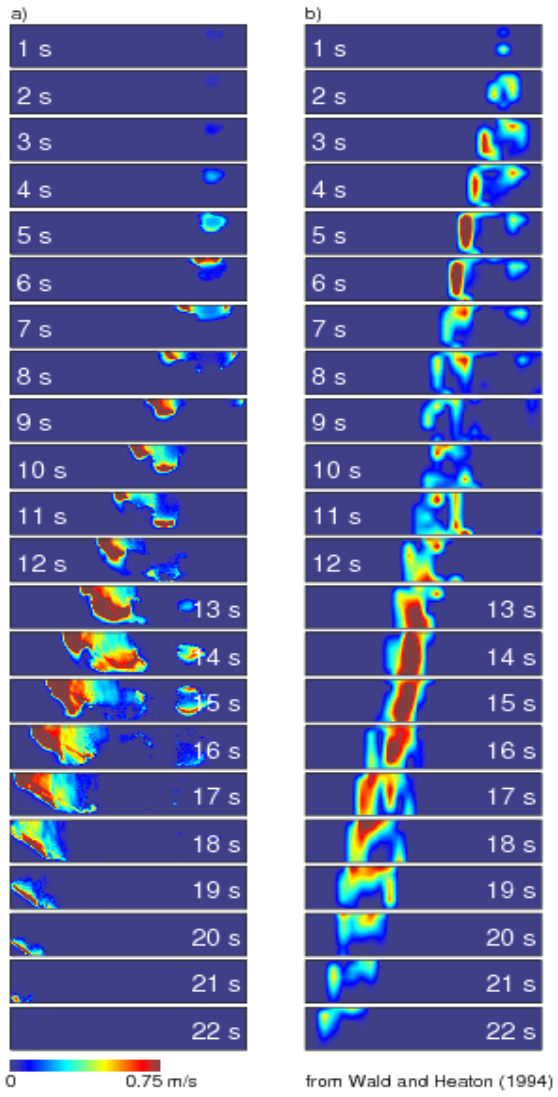

Figure 8: Snapshots of the dynamic rupture simulation of the Landers earthquake compared with a kinematic inversion by Wald and Heaton (1994). The snapshots depict the horizontal slip rate where hotter colours depict larger values.

6. DISCUSSION AND CONCLUSION

Initial models of dynamic rupture propagation (e.g., Andrews, 1976, Madariaga, 1976, Das and Aki, 1977) studied the frictional instability of a uniformly loaded fault. Very rapidly it was realized that heterogeneity was an essential ingredient of seismic ruptures and that the simple uniformly loaded faults could not explain many significant features of seismic radiation. Two models of heterogeneity were proposed in the late 70s, the asperity model of Stewart and Kanamori (1978) based on a study of the Guatemalan earthquake of 1976 and the barrier model of Das and Aki (1977b). The differences between the two models were discussed in some detail by Madariaga (1979) who pointed out that it would be very difficult to distinguish between these two models from seismic observations alone. This remains true today. In the asperity model, it is assumed that the initial stress field is very heterogeneous because previous events have left the fault in a very complex state of stress. In the barrier model, heterogeneity is produced by rapid changes in rupture resistance so that an earthquake would leave certain patches of the fault (barriers) unbroken. It was quickly realized that barriers and asperities were necessary in order to maintain a certain degree of heterogeneity on the fault plane that could explain the properties of high frequency seismic wave radiation and to leave highly stressed patches that would be the sites of aftershocks and future earthquakes.

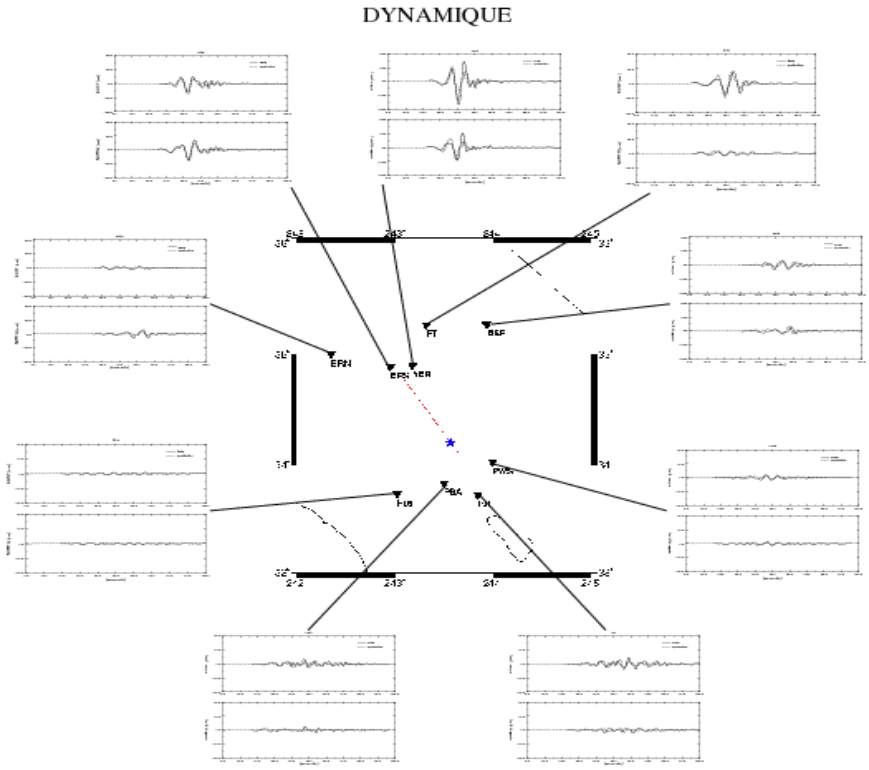

Figure 9: Comparison of simulated (dashed) to observed (solid) seismograms at several accelerometric stations around the Landers earthquake.

Thanks to improvements in speed and memory of parallel computers it is no longer a problem to simulate seismic ruptures propagating along a fault, or set of faults, embedded in an elastic 3D body. This new capability could be used to improve classical models in order to determine the grid size necessary to do reproducible and stable earthquake simulations. We showed that the conditions are that the slip-weakening zone near the rupture front must be sampled by more than 7 grid points. This is an exacting condition but it is already possible to model earthquakes up to 7.5 without insurmountable problems. Dynamic inversion, on the other hand, requires thousands of simulations that are still difficult to do in computer clusters in a reasonable time.

Recent inversions of earthquake slip distributions using kinematic source models have found very complex source distributions require an extensive reappraisal of classical source models that were mostly based on

Kostrov's model of self-similar circular crack. Ruptures in a fault with a very heterogeneous load follow very tortuous rupture paths. While on the mean the rupture propagates at a sub-sonic speed from one end of the fault to another, in detail the rupture front can wander in all directions following the areas of strong stress concentration and avoiding those with low stress or high rupture resistance. If this view of earthquake rupture was to be confirmed by future observations (we believe it will be) then many current arguments about earthquake complexity, narrow rupture pulses, earthquake distributions, will be solved and we may concentrate on the truly interesting problem of determining which features of friction determine that fault stress is always complex under all circumstances.

ACKNOWLEDGEMENTS

This work was supported by the European Commission under the Spice research and training network and by project ANR CATELL 2005 “Seismic simulation in the complex source-site contexts (SEISMULATORS)”

REFERENCES

Andrews, J. (1976). Rupture velocity of plane strain shear cracks, J. Geophys. Res. 81, 5679-5687. .

Andrews, D. J., Test of two methods for faulting in finite-difference calculation. Bull. Seismol. Soc. Am. 89, 931-937. 1999.

Bizzarri, A., M. Cocco, D. J. Andrews and E. Boschi (2001). Solving the dynamic rupture problem with different numerical approaches and constitutive laws, Geophys. J. Int., 144, 656-678.

Bouchon, M. (1981) A simple method to calculate Green's functions for elastic layered media. Bull. Seismol. Soc. A., 71, 959-971.

Bouchon, M. (1997). The state of stress on some faults of the San Andreas system as inferred from near-field strong motion data, Jour. Geophys. Res. 102,11731-11744.

Brune,J.(1970). Tectonic stress and the spectra of seismic shear waves from earthquakes,J. Geophys. Res. 75, 4997-5009.

Cochard, A., and Madariaga, R. (1994). Dynamic faulting under rate-dependent friction, Pageoph 142, 419-445.

Cohee, B., and Beroza, G. (1994). Slip distribution of the 1992 Landers earthquake and its implications for earthquake source mechanics, Bull. Seis. Soc. Am. 84, 692-712.

Cotton, F., and Campillo, M. (1995). Frequency domain inversion of strong motions: application to the 1992 Landers earthquake, J. Geophys. Res. 100, 3961-3975.

Das, S., and Aki, K. (1977). A numerical study of two-dimensional spontaneous rupture propagation, Geophys. J. Roy. astr. Soc., 50, 643-668.

Das, S .(1980). A numerical method for the estimation of source time functions for general three-dimensional rupture propagation, Geophys. J. Roy. astr. Soc., 62, 591-604.

Das, S., and Kostrov, D.(1983). Breaking of a single asperity: Rupture process and seismic radiation. J. Geophys. Res. 88, 4277-4288.

Day, S. M. (1982). Three-dimensional simulation of spontaneous rupture: the effect of non-uniform prestress, Bull. Seis. Soc. Am. 72, 1881-1902.

Day, S., Dalguer, L.A., Lapusta, N., Liu, Y. (2005) Comparison of finite difference and boundary integral solutions to three-dimensional spontaneous rupture, J. Geophys. Res, B110, B12307.1-B12307.23.

Dieterich, J. (1978). Time-dependent friction and the mechanics of stick-slip, Pageoph 116, 790-806.

Fukuyama, E., and Madariaga, R. (1998). Rupture dynamics of a planar fault in a 3D elastic medium: Rate-and slip-weakening friction, Bull. Seismol. Soc. Am. 88, 1-17.

Haskell, N.A. (1964). Total energy spectral density of elastic wave radiation from propagating faults, Bull. Seismol. Soc. Am. 54, 1811-1841.

Heaton,T.(1990). Evidence for and implications of self-healing pulses of slip in earthquake rupture, Phys. Earth. Planet. Int. 64, 1-20.

Ida, Y. (1972). Cohesive force across the tip of a longitudinal-shear crack and Griffith's specific surface energy, J. Geophys. Res. 77, 3796-3805.

Ide, S.,and Takeo,M.(1997). Determination of the constitutive relation of fault slip based on wave analysis, J. Geophys. Res. 102, 27379-27391.

Kanamori, H. and Stewart, G.S. (1976), Seismological aspects of the Guatemala earthquake of February 4, 1976, J. Geophys. Res. 83, 3427-3434.

Koller, M. G., Bonnet, M. and Madariaga, R. (1992). Modelling of dynamical crack propagation using time-domain boundary integral equations, Wave Motion, 16, 339-366.

Komatitsch, D., J-P. Vilotte, (1998). The spectral element method: An efficient tool to simulate the seismic response of 2D and 3D geological structures. Bull. Sismol. Soc. Am.,88, 368-392.

Kostrov, B. (1964). Self-similar problems of propagation of shear cracks, J. Appl. Math. Mech. 28, 1077-1087.

Kostrov, B. and Das, S. (1989). Principles of Earthquake Source Mechanics, Cambridge University Press.

Madariaga, R. (1976). Dynamics of an expanding circular fault, Bull. Seismol. Soc. Am.66, 639-667.

Madariaga, R., (1979), On the relation between seismic moment and stress drop in the presence of stress and strength heterogeneity, J. Geophys. Res. 84, 2243-2250.

Madariaga, R., Olsen, K.B., and Archuleta, R.J. (1998). Modelling dynamic rupture in a 3D earthquake fault model, Bull. Seismol. Soc. Am. 88, 1182-1197.

Madariaga, R. and Ampuero, J.P. (2005) Rupture dynamics of a geometrically complex fault. AGU Fall Meeting Abstracts,

Olsen, K., Archuleta, R. and Matarese, J. (1995). Three-dimensional simulation of a magnitude 7.75 earthquake on the San Andreas fault, Science 270, 1628-1632.

Olsen,K., Madariaga,R. and Archuleta,R. (1997). Three dimensional dynamic simulation of the 1992 Landers earthquake, Science 278, 834-838.

Peyrat, S., Olsen K.B. and Madariaga,R. (2001). Dynamic modelling of the 1992 Landers Earthquake, submitted to J. Geophys. Res. 106, 25467-25482.

Ruina, A. (1983). Slip instability and state variable friction laws, J. Geophys. Res. 88, 10359-10370.

Scholz,C.(1989). The Mechanics of Earthquake and Faulting, Cambridge University Press.

Wald, D. and Heaton, T. (1994). Spatial and temporal distribution of slip for the 1992 Landers, California earthquake, Bull. Seis. Soc. Am. 84, 668-691.